ACS NANO
Cite This: ACS Nano 2018, 12, 6100−6108
www.acsnano.org

ARTICLE

van der Waals Epitaxy of Antimony Islands, Sheets, and Thin Films on Single-Crystalline Graphene

Xin Sun,*[,†] Zonghuan Lu,[†] Yu Xiang,[†] Yiping Wang,[‡] Jian Shi,[‡] Gwo-Ching Wang,[†] Morris A. Washington,[†] and Toh-Ming Lu[†]

[†]Center for Materials, Devices and Integrated Systems and Department of Physics, Applied Physics and Astronomy, and [‡]Department of Materials Science and Engineering, Rensselaer Polytechnic Institute, Troy, New York 12180, United States

Supporting Information

ABSTRACT: Antimony (Sb) nanostructures, including islands, sheets, and thin films, of high crystallinity were epitaxially grown on single-crystalline graphene through van der Waals interactions. Two types of graphene substrates grown by chemical vapor deposition were used, the as-grown graphene on Cu(111)/*c*-sapphire and the transferred graphene on SiO_2/Si. On the as-grown graphene, deposition of ultrathin Sb resulted in two growth modes and associated morphologies of Sb. One was Sb islands grown in Volmer−Weber (VW) mode, and the other was Sb sheets grown in Frank−van der Merve (FM) mode. In contrast, only Sb islands grown in VW mode were found in a parallel growth experiment on the transferred graphene. The existence of Sb sheets on the as-grown graphene was attributed to the remote epitaxy between Sb and Cu underneath the graphene. In addition, Sb thin films were grown on both the as-grown and transferred graphene substrates. Both films indicated high quality, and no significant difference can be found between these two films. This work unveiled two epitaxial alignments between Sb(0001) and graphene, namely, Sb $[10\bar{1}0]$‖graphene [10] for Sb islands and Sb $[2\bar{1}\bar{1}0]$‖graphene [10] for Sb sheets. For Sb thin films on graphene, the epitaxial alignment followed that of Sb islands, implying that Sb thin films originated from the continued growth of Sb islands. Last, Raman spectroscopy was used to probe the state of graphene under ultrathin Sb. No strain, doping, or disorder was found in the graphene postgrowth of Sb. The knowledge of the interface formation between ultrathin Sb and graphene provides a valuable foundation for future research on van der Waals heterostructures between antimonene and graphene.

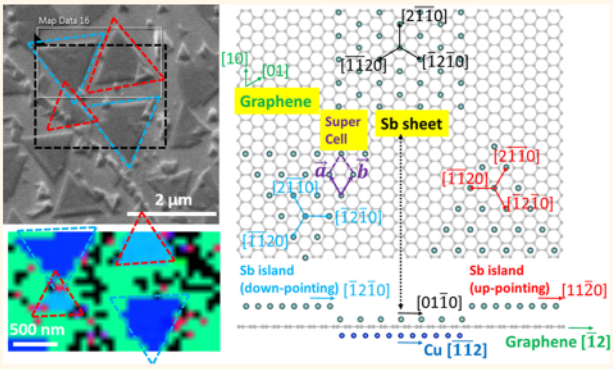

KEYWORDS: *van der Waals epitaxy, antimony, graphene, growth mode, crystallography, electron backscatter diffraction*

Due to the predicted stability, electronic and optical properties, and the potential for topological phase transitions, ultrathin Sb, in particular, monolayered or the so-called antimonene, has attracted attention.[1−6] Although most investigations on this topic are confined to density functional theory (DFT) at this point, several reputable experimental works have recently emerged, as well. In addition to mechanical and liquid-phase exfoliation methods, vapor-phase epitaxy of ultrathin Sb has been demonstrated on a variety of substrates, including mica, $PdTe_2$, Sb_2Te_3, Bi_2Te_3, Bi_2Te_2Se, Ag, and Ge.[7−14] However, the growth of ultrathin Sb on graphene, arguably the most attractive 2D material, has not been reported yet. We believe this endeavor is worth exploring because it would generate a great deal of interests for the following reasons.

First, if monolayer Sb is really a semiconductor with tunable band gap as predicted by theory, the van der Waals heterostructure of Sb−graphene would be of great use for optoelectronics (photovoltaics, photodetectors, and light-emitting diodes) where graphene serves the function of electrodes.[15,16] This prospect sounds even more exciting if put in the context of flexible electronics because graphene is truly transferrable, transparent, stable, and wearable. Second, graphene has become a scalable material with low cost of production, as researchers put in enormous efforts to make it practically useful.[17] Thus, graphene has a substantial advantage over other options as the substrate for Sb heterostructures

Received: March 29, 2018
Accepted: May 10, 2018
Published: May 10, 2018

DOI: 10.1021/acsnano.8b02374
ACS Nano 2018, 12, 6100−6108

Table 1. Summary of Various Sb Nanostructures on As-Grown and Transferred Graphene Substrates

deposition thickness (QCM)	substrate	morphology	epitaxial alignment	
			plane	direction
10 nm	as-grown graphene	island	Sb(0001)‖graphene	primary island: Sb [10$\bar{1}$0]‖graphene [10] twin island: Sb [1$\bar{1}$00]‖graphene [10]
		sheet	Sb(0001)‖graphene‖Cu(111)	Sb [2$\bar{1}\bar{1}$0]‖graphene [10]‖Cu [1$\bar{1}$0]
10 nm	transferred graphene	island	Sb(0001)‖graphene	N/A[a]
300 nm	as-grown graphene	thin film	Sb(0001)‖graphene	primary domain: Sb [10$\bar{1}$0]‖graphene [10] twin domain: Sb [1$\bar{1}$00]‖graphene [10]
300 nm	transferred graphene	thin film	Sb(0001)‖graphene	primary domain: Sb [10$\bar{1}$0]‖graphene [10] twin domain: Sb [1$\bar{1}$00]‖graphene [10]

[a]No direct experimental evidence was collected. It is speculated to be the same as that for the 300 nm Sb thin film on a transferred graphene.

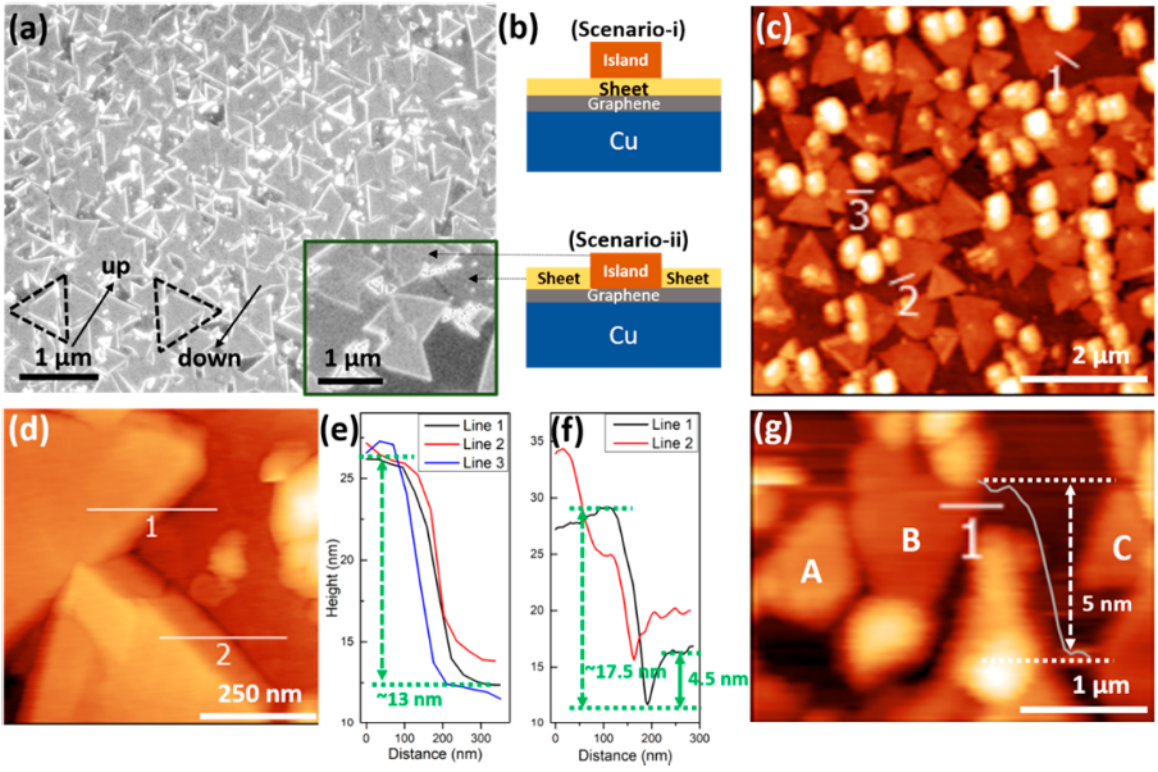

Figure 1. SEM image of 10 nm Sb deposited on an as-grown graphene substrate at 150 °C. The image shows two types of Sb triangle islands, one pointing up and one pointing down, as labeled by the dashed triangles. Together they account for the major fraction in the image. Inset: SEM image of a selected area comparing Sb islands (gray shade), Sb sheets (gray shade), and blank surface (black shade). (b) Side view schematics illustrating two possible configurations of Sb islands (brown) and sheets (yellow) on graphene (gray). Top: scenario-i. Bottom: scenario-ii. (c) AFM image of a large area scan of 10 nm Sb deposited on an as-grown graphene. (d) AFM image of a small area scan of 10 nm Sb deposited on an as-grown graphene, focusing on the boundaries between Sb islands and sheets. (e,f) Line scan profiles of the lines shown in (c) and (d), respectively. (g) AFM image of 3 nm Sb deposited on an as-grown graphene at 150 °C.

when it comes to scale-up and integration with standard integrated circuit technology. Last, from the perspective of surface science, Sb has traditionally been known as an effective surfactant to adjust the wettability of materials.[18−24] For graphene, there happens to be a real need to find an effective way to wet it because it has an extremely low surface tension.[25,26] Given the relatively lower surface tension of Sb compared to that of other materials, it may be possible for Sb to grow on graphene in Frank−van der Merve (FM) fashion. If so, a buffer of ultrathin Sb would allow the subsequent growth of thin films on graphene in a desired structure. To pursue this idea, it is necessary to experiment how Sb grows on graphene in the first place.

In this work, two types of chemical vapor deposited (CVD) single-crystalline graphene, namely, the as-grown graphene on Cu(111)/*c*-sapphire and the transferred graphene on SiO_2(50 nm)/Si, were used for epitaxy of Sb. The growth mode of Sb, either Volmer−Weber (VW), FM, or both, on graphene was systematically investigated. Crystallographic investigations using electron backscatter diffraction (EBSD) and X-ray diffraction (XRD) were employed to probe the crystallinity of the Sb on both graphene substrates (as-grown and transferred), regardless whether the Sb was in island, sheet, or thin film morphology. Moreover, two epitaxial alignments between Sb and graphene, including one as a result of remote epitaxy between Sb and Cu, were concluded from the crystallographic study, which provides a better understanding on the interface

DOI: 10.1021/acsnano.8b02374
ACS Nano 2018, 12, 6100−6108

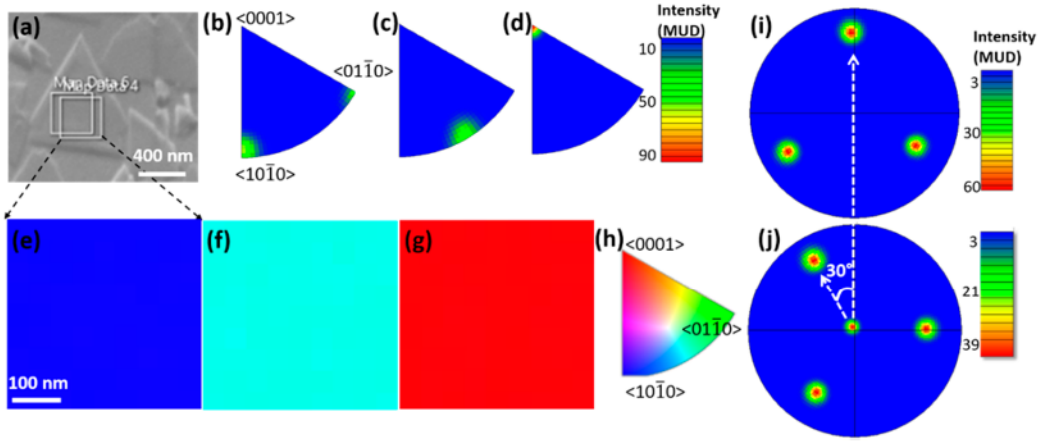

Figure 2. (a) SEM image (obtained with the EBSD system) of 10 nm Sb deposited on an as-grown graphene substrate at 150 °C, focusing on a single Sb island. Note that in the image there are two white squares indicating the selected areas for EBSD mapping. The top-left white square was initially selected, but the scan area shifted during the data acquisition. As a result, the second attempt, indicated by the bottom-right white square, was performed. Thus, the area confined by the bottom-right square represents the actual area for the EBSD measurement. (b–d) EBSD inverse pole figure (IPF) of the white square area along *X*, *Y*, and *Z* directions, respectively. (e–g) EBSD crystallographic orientation mappings using IPF-*X*, IPF-*Y*, and IPF-*Z*, respectively, of the white square area. (h) Color code for the mappings in (e–g). (i) EBSD pole figure of Sb (10$\bar{1}$1) collected from the white square area. (j) EBSD pole figure of Cu (111) collected from an area without Sb coverage. The white dashed lines show the offset angle between poles in (i) and (j).

engineering of Sb–graphene and Sb–graphene–Cu heterostructures. A quick summary of the results is listed in Table 1.

RESULTS AND DISCUSSION

Morphology of Sb Islands and Sheets on the As-Grown Graphene. Figure 1a shows a scanning electron microscopy (SEM) image of 10 nm thick, according to a quartz crystal microbalance (QCM), Sb deposited on an as-grown graphene at 150 °C. The main feature observed in this image is the triangle islands aligned along certain directions. The preferred alignment, in spite of some dispersion, suggests epitaxy growth, which will be confirmed by EBSD and XRD data later. The islands show two major orientations that are 60° apart from each other, indicated by the dashed triangles in Figure 1a, one pointing up and the other pointing down (equivalent to a 60° in-plane twinning rotation of the former). The side length of islands varies from 200 nm to 1 μm. Inset of Figure 1a focuses on a local area of this sample. The image contrast suggests that Sb also forms sheets in addition to islands. Explicitly, both Sb sheets and islands are represented by the gray shaded areas. An area without Sb coverage should be in black under SEM, as shown by the lower-right part of this inset image. Based on these observations, there are two possible scenarios for Sb to grow on an as-grown graphene, schematically explained in Figure 1b. In scenario-i, it is likely that Sb forms a large and almost full-coverage sheet on graphene first, followed by the formation of Sb islands on top of the Sb sheet. In scenario-ii, Sb islands and sheets grow on graphene simultaneously but separately, and they form boundaries when meeting each other.

To probe this difference further, atomic force microscopy (AFM) was used, which gives the quantitative height information on Sb islands and sheets. Figure 1c shows a large-area AFM scan, where the average height of three individual Sb islands is shown to be ~13 ± 2 nm by the line scans in Figure 1e. Note that the boundaries, if they exist between islands and sheets, cannot be resolved in this scale. Thus, this height of a Sb island is a relative value with respect to a Sb sheet. To further determine if the boundaries exist, a high-resolution AFM scan was measured, shown in Figure 1d, where gaps between Sb islands and the surrounding Sb sheet are confirmed. The two line scan profiles in Figure 1f indicate that the absolute height of Sb islands is ~17.5 ± 0.7 nm, and the height of Sb sheets is ~4.5 ± 0.7 nm. These values are consistent with the relative heights of Sb islands with respect to sheets obtained from Figure 1e. It thus suggests that the second case shown in Figure 1b might be valid to describe this growth, which hints two growth modes adopted when Sb grows on an as-grown graphene. That is, Sb islands take the VW growth mode, and Sb sheets take the FM growth mode. Initially, they nucleate and grow independently. As the dimensions increase, these two nanostructures meet and merge together. The AFM image in Figure 1d represents a moment that they have not merged yet.

Figure 1g shows the AFM image of smaller Sb islands when the deposition thickness was cut down to 3 nm (QCM), with all other conditions the same as those in Figure 1c,d. It can be seen that Sb islands, labeled in A, B, and C, maintain the triangular geometry. The height profile for line 1 indicates the height of Sb island B is reduced to 5 nm, equivalent to few-layered antimonene. At this growth stage, the Sb sheets are speculated to be very thin. The regular scanning probe microscopic technique, that is, AFM here, cannot tell if or where these thin Sb sheets exist.

Morphology of Sb Islands on the Transferred Graphene and Highly Oriented Pyrolytic Graphite. In contrast, only VW growth of Sb, in island form, can be found when the same deposition process was conducted on a transferred graphene, as shown in Figure S1a. The absence of Sb sheets, which will be confirmed later, on a transferred graphene suggests that the formation of Sb sheets on an as-grown graphene may be caused by the underlying Cu. Without Cu, Sb intrinsically tends to form islands on graphene. One may argue that the large amount of defects in transferred graphene may introduce uncertainties and thus make this comparison unfair. To remove this suspicion, a freshly cleaved highly oriented pyrolytic graphite (HOPG), with much fewer defects than transferred graphene, was also used as a substrate

DOI: 10.1021/acsnano.8b02374
ACS Nano 2018, 12, 6100–6108

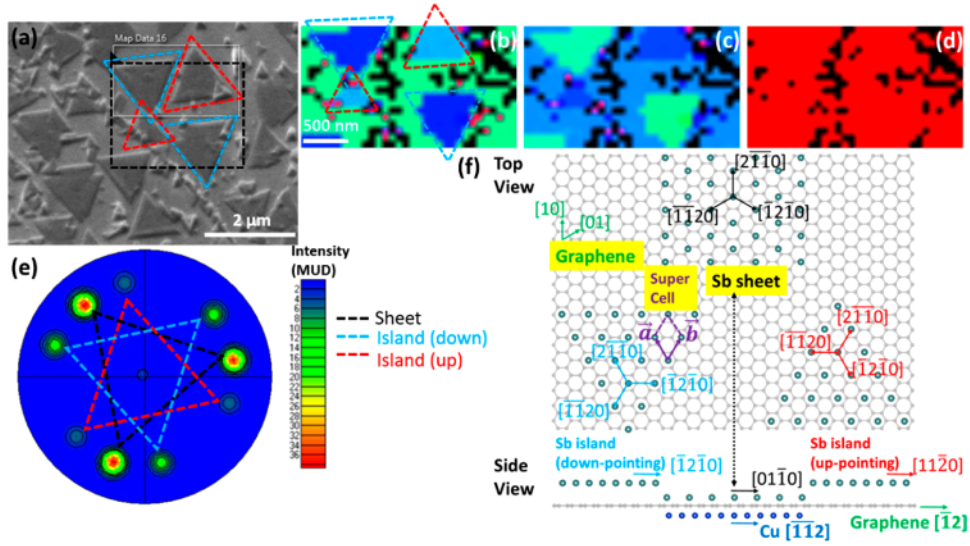

Figure 3. (a) SEM image (obtained with the EBSD system) of 10 nm Sb deposited on an as-grown graphene substrate at 150 °C, covering more Sb islands and sheets for relative orientation study. The black dashed rectangle represents the actual selected area for the EBSD measurement. (b–d) EBSD crystallographic orientation mappings using IPF-*X*, IPF-*Y*, and IPF-*Z*, respectively, of the black dashed rectangle area. The color code is the same as that of Figure 2h. (e) EBSD pole figure of Sb (10$\bar{1}$1) collected from the black dashed rectangle area. Three sets of three-fold symmetrical poles corresponding to the three Sb features in (b–d). (f) Atomic models showing the alignments of three types of Sb features on a single-crystalline graphene template. The drawing in this graph is scaled with the actual in-plane lattice ratio of Sb to graphene.

for Sb deposition. It is found that the HOPG surface was extremely difficult to wet. The deposition duration had to be prolonged 10 times before Sb products were finally obtained. As shown in Figure S1b, Sb takes the VW growth mode by forming islands on HOPG. This piece of evidence further adds weight to the judgment that Sb tends to form islands on graphene if there is no Cu underneath graphene. This conclusion vetoes our expectation of using Sb to wet pristine graphene based on the fact that Sb has a relatively low surface tension in comparison to other materials. In fact, this negative result is not unreasonable. Despite a relatively low surface tension in Sb, it is still higher than the surface tension of pristine graphene, making the wetting of the former on the latter challenging.

The similar role that supporting substrates underlying graphene play on the growth of overlayers has also been observed elsewhere. For example, an enhancement in Al_2O_3 nucleation density on graphene was found when switching the graphene support from SiO_2 to Cu.[27] The effect was attributed to a polar trapping mechanism, though it does not fit our case of Sb on graphene because Sb is nonpolar. It has also been reported that the growth mode of pentacene film on graphene can be changed by tuning the wettability of the supporting SiO_2 surface using different plasma treatments.[28] These evidence, along with the present study, suggests that graphene cannot fully screen the interaction coming from the supporting substrates, which can remotely mediate the growth behaviors of overlayers through graphene.

EBSD Crystallography of Sb Islands and Sheets on the As-Grown Graphene. To investigate the crystallinity and orientation of Sb islands grown on the as-grown graphene at 150 °C shown in Figure 1a, EBSD was conducted on a single piece of Sb island. The selected area for this scan is shown by the bottom-right square in Figure 2a. EBSD confirms that the island matches with the crystallography information on rhombohedral β-Sb in the ICSD database as follows: space group 166, $a = b = 4.30$ Å, $c = 11.23$ Å, and $\alpha = \beta = 90°$, $\gamma = 120°$. For this Sb island, the inverse pole figures (IPF) along *X*, *Y*, and *Z* directions shown in Figure 2b–d indicate that the out-of-plane orientation is ⟨0001⟩, and the in-plane orientations are ⟨10$\bar{1}$0⟩ and ⟨11$\bar{2}$0⟩. Ideally, the pole in IPF-*X* (Figure 2b) should be localized at the ⟨10$\bar{1}$0⟩ corner. However, there is a small shift due to the spread of crystal in-plane alignment. Figure 2e–g shows the crystallographic orientation mappings using the IPF-*X*, IPF-*Y*, and IPF-*Z* components, respectively, where perfectly homogeneous color is found in each. It means that the crystallinity of this Sb island is nearly perfect. According to the color code in Figure 2h, the out-of-plane and in-plane orientations are consistent with the previous assignment in Figure 2b–d. To determine the alignment between this Sb island and graphene, the EBSD pole figure of Sb (10$\bar{1}$1) was collected, as shown in Figure 2i. A sharp three-fold symmetry can be seen, and it confirms the single crystallinity of this Sb island. On this sample, the EBSD (111) pole figure of the underlying Cu(111) was also collected, as shown in Figure 2j, which is a set of three-fold symmetrical poles resulting from the single-crystalline Cu. It is shown in Figure 2i,j that there is a 30° offset between Sb (10$\bar{1}$1) and Cu(111) poles. Based on this, the alignment between Sb and Cu can be deduced as Sb(0001)‖Cu(111) and Sb [10$\bar{1}$0]‖Cu [1$\bar{1}$0]. According to our previous work, the graphene is epitaxially grown on Cu(111) with the following alignment: graphene [10]‖Cu [1$\bar{1}$0].[29] Thus, the epitaxial alignment between this Sb island and graphene can be concluded as Sb [10$\bar{1}$0]‖graphene [10]. See Table 1.

As pointed out earlier, there are three forms of Sb in the sample shown in Figure 1a, namely, up-pointing triangle islands, down-pointing triangle islands (equivalent to a 60° in-plane twinning rotation of the former), and sheets between islands. To learn more about their differences and relations in terms of crystallography, the EBSD scan area was enlarged to cover them all. A scan area, indicated by the white solid

DOI: 10.1021/acsnano.8b02374
ACS Nano 2018, 12, 6100–6108

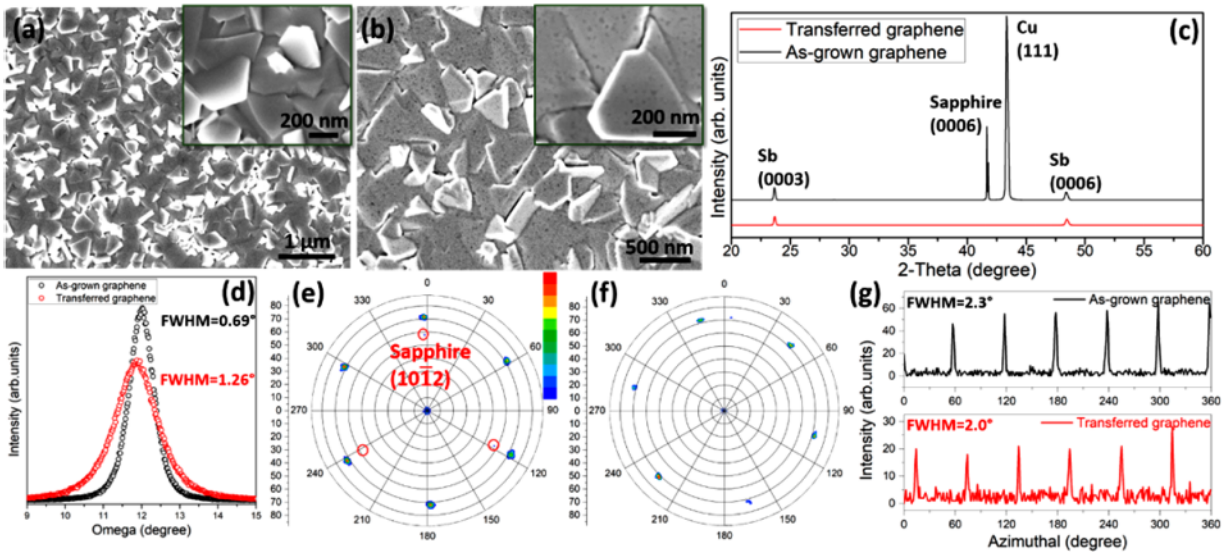

Figure 4. Sb thin films (300 nm thick) grown on an as-grown graphene substrate and a transferred graphene substrate at 150 °C. (a) SEM image of Sb film on as-grown graphene. Inset: higher magnification of (a). (b) SEM image of Sb film on transferred graphene. Inset: higher magnification of (b). (c) XRD θ–2θ scans of both Sb films showing a dominating (0001) out-of-plane orientation. (d) XRD rocking curves of Sb (0003) diffractions for both Sb films. (e) X-ray pole figure of Sb (10$\bar{1}$1) showing six-fold symmetry of Sb film on as-grown graphene. Additional three symmetrical poles in red circles attributed to sapphire (10$\bar{1}$2). (f) X-ray pole figure of Sb (10$\bar{1}$1) showing six-fold symmetry of Sb film on transferred graphene. (g) XRD azimuthal scans of Sb (10$\bar{1}$1) for both Sb films.

rectangle in Figure 3a, was purposely selected to cover a pair of the opposite-pointing triangle islands and the sheet between them. Due to the image shifting, the actual scan area, indicated by the black dashed rectangle, was slightly different from targeted area (white solid rectangle), but it does not affect the result. The IPF orientation mappings along *X*, *Y*, and *Z* directions for this scan are shown in Figures 3b–d. The black spots coming from the zero resolution of the EBSD system due to the surface scattering can be ignored. In Figure 3b,c, three colors corresponding to three orientations are found in the three features of Sb, meaning the in-plane orientations of up-pointing islands, down-pointing islands, and sheets are different. Figure 3d suggests the out-of-plane orientation is ⟨0001⟩ for all forms of Sb. It should be emphasized that this EBSD mapping provides a strong evidence that Sb sheets exist between islands, which may have been overlooked if using only imaging tools such as SEM and AFM. It should also be emphasized that this EBSD mapping confirms the separate and simultaneous growth of Sb islands and sheets, consistent with the schematic shown in the scenario-ii of Figure 1b. If Sb islands sit on Sb sheets as shown in the scenario-i of Figure 1b, no Kikuchi pattern can be resolved at those island regions because there would be two different crystallographic orientations under the probing area, and the EBSD mapping on those islands would result in zero resolution.

To reveal the in-plane rotations among up-pointing islands, down-pointing islands, and sheets, the EBSD pole figure of Sb (10$\bar{1}$1) was constructed in Figure 3e. Three sets of Sb (10$\bar{1}$1) poles, separated by 30°, can be found, corresponding to the three forms of Sb. Note that the in-plane offset angle between up-pointing and down-pointing islands obviously should be 60°. Essentially, these two types of islands are twins to each other. Based on this, the middle set of poles (black dashed lines) can be attributed to Sb sheets which rotate ±30° from the Sb islands. The set of poles with the moderate intensity (blue dashed lines) is likely from the down-pointing islands because those islands account for more coverage than up-pointing islands in the scan area. That leaves the last set of poles (red dashed lines) to up-pointing islands. Also note that the EBSD measurements in Figures 2 and 3 were not conducted at the same time. In other words, the sample's *X* and *Y* directions, depending on how the samples were mounted, were not the same. This caused the inconsistency in assignments of mapping color and pole rotation in EBSD. However, this will not affect the conclusions drawn from an individual EBSD scan. Based on the previously established alignment between one type of Sb island and graphene in Figure 2, a complete set of alignment between Sb (up-pointing islands, down-pointing islands, and sheets) and graphene can be unveiled. As shown in Figure 3f, in both top and side views, Sb sheets align with graphene as Sb [2$\bar{1}\bar{1}$0]‖graphene [10], down-pointing Sb islands align with graphene as Sb [10$\bar{1}$0]‖graphene [10] (same as the island in Figure 2), and up-pointing Sb islands align with graphene as Sb [1$\bar{1}$00]‖graphene [10]. See Table 1. Note that the scale in Figure 3f is adjusted to match the real space lattice ratio between Sb and graphene. It can be found from the top view that the Sb atoms in islands nicely fit into the carbon rings in graphene, but it is not the case for the atoms in Sb sheets on graphene. This may indicate that the Sb island formation on graphene is more energetically favorable. Quantitively, this favorability can be interpreted by the super cell formed between down-pointing Sb island and graphene, shown by the purple cell in Figure 3f. In this super cell, the $\vec{a}$ and $\vec{b}$ of Sb are [2$\bar{1}\bar{1}$0] and [11$\bar{2}$0], respectively; and the $\vec{a}$ and $\vec{b}$ of graphene are [2$\bar{1}$] and [11], respectively. The lattice mismatch for this super cell is calculated to be 1.17%. Such a small lattice mismatch is believed to be the reason that Sb islands aligned on graphene in this direction would be more stable, which will be confirmed in the following study of Sb thin films.

EBSD Crystallography of Sb Islands on the Transferred Graphene. EBSD mapping was also conducted on those Sb islands formed on the transferred graphene. Figure S2 shows the selected area covering several Sb islands and the

DOI: 10.1021/acsnano.8b02374
ACS Nano 2018, 12, 6100–6108

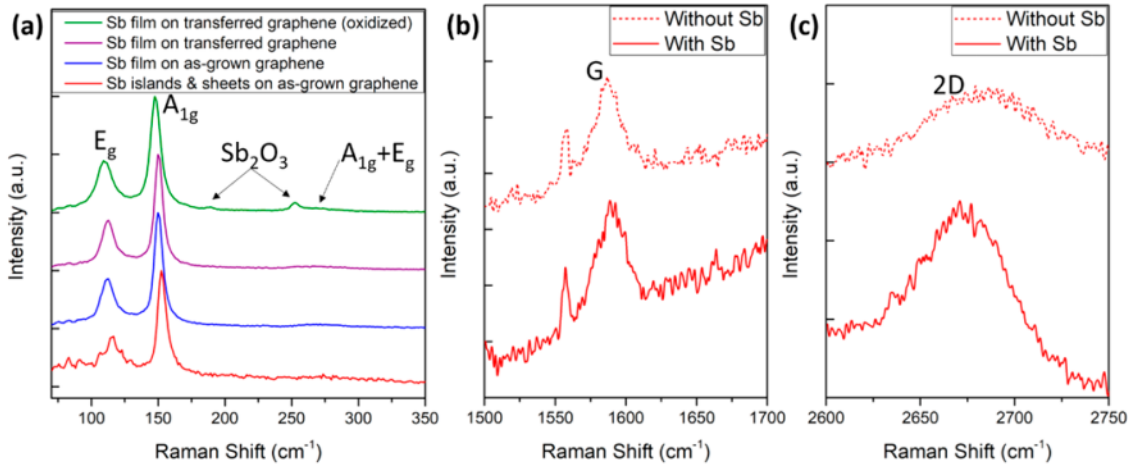

Figure 5. (a) Room temperature Raman spectra of three kinds of Sb samples: Sb islands and sheets on as-grown graphene, Sb thin film on an as-grown graphene, and Sb thin film on a transferred graphene. (b) G peak of graphene obtained from the Sb islands and sheets on an as-grown graphene sample. Solid curve: spectrum obtained from an area covered by Sb. Dashed curve: spectrum obtained from an area not covered by Sb. The sharp peak around 1557 cm^{-1} comes from an artifact. (c) 2D peak of graphene obtained from the Sb islands and sheets on an as-grown graphene sample. Solid curve: spectrum obtained from an area covered by Sb. Dashed curve: spectrum obtained from an area not covered by Sb.

corresponding crystallographic mappings along the sample's *X*, *Y*, and *Z* directions. Due to the small dimension of Sb islands, the EBSD system with a lateral resolution of ~75 nm cannot resolve the geometry of Sb islands, but that will not hinder the most important learning from this scan; that is, no Sb sheets form between Sb islands on the transferred graphene. With this evidence, it can be concluded that the formation of Sb sheets on the as-grown graphene is purely induced by the underlying Cu, likely through the remote epitaxy mechanism,[30] confirming that graphene is at least partially transparent in our case. Now, the complete epitaxial alignment for Sb sheets should be extended as follows: Sb(0001)||graphene||Cu(111) and Sb $[2\bar{1}\bar{1}0]$||graphene [10]||Cu $[1\bar{1}0]$ (equivalently, Sb $[01\bar{1}0]$||graphene $[\bar{1}2]$||Cu $[\bar{1}\bar{1}2]$ as shown in the side view of Figure 3f). One may suspect that the epitaxy of Sb islands on the as-grown graphene is also a remote epitaxy between Sb and Cu; in other words, graphene is fully transparent. While such a possibility cannot be excluded, we will demonstrate in the Sb Thin Films on the Transferred Graphene section that transferred graphene itself indeed can induce an epitaxy of Sb, and the epitaxial alignment of Sb on transferred graphene is the same as that of Sb islands on the as-grown graphene. Thus, the epitaxial growth of Sb islands on the as-grown graphene is, at least partially, contributed by graphene.

Sb Thin Films on the As-Grown Graphene. In addition to the ultrathin Sb products just described, thicker Sb films on as-grown and transferred graphene were also studied. Figure 4a shows a SEM image of a 300 nm thick Sb film deposited on as-grown graphene at 150 °C. Sharp crystal facets can be seen in this image and a high-magnification image in the inset of Figure 4a, indicating a high crystallinity of the thin film. The XRD θ–2θ scan in Figure 4c suggests that the film is (0001) oriented along the out-of-plane direction, same as that of Sb islands and sheets. Cu(111) and sapphire (0006) peaks can also be identified in the scan. Figure 4d exhibits the rocking curve of Sb (0003) diffraction with a full width at half-maximum (fwhm) of 0.69°, suggesting the spread of Sb grains in the out-of-plane direction is very small.

To reveal the in-plane orientation of this film, the X-ray pole figure of Sb $(10\bar{1}1)$ was collected at 2θ = 25.12°. The pole figure in Figure 4e shows six sharp and symmetrical poles at a polar angle of χ = 72°. As shown earlier by EBSD, the Sb $(10\bar{1}1)$ pole figure should show three-fold symmetry for a perfect single crystal. The six-fold symmetry shown in Figure 4e suggests the coexistence of two twinned domains that are rotated 60° in-plane with respect to each other. Note that additional three-fold symmetrical poles are found at χ = 58° in Figure 4e, matching very well to sapphire $(10\bar{1}2)$ poles whose 2θ = 25.58° and χ = 58° in its (0001) polar stereographic projection. The existence of this set of sapphire poles is fortunate that it allows us to determine the in-plane alignment between Sb film and graphene using a similar method applied in Figure 2i,j. Based on the pole alignment in Figure 4e, it can be deduced that one of the twinned domains in this Sb film is aligned with sapphire as follows: Sb(0001)||sapphire(0001) and Sb $[10\bar{1}0]$||sapphire $[10\bar{1}0]$. According to our previous work, sapphire is aligned with Cu and graphene as follows: graphene||Cu(111)||sapphire(0001) and graphene [10]||Cu $[1\bar{1}0]$||sapphire $[10\bar{1}0]$.[29] Given these two alignments, it can be concluded that one of the twinned domains in Sb film is aligned with graphene as Sb $[10\bar{1}0]$||graphene [10]. See Table 1. This alignment is the same as that between the down-pointing Sb islands and graphene shown in Figure 3f. Apparently, the other domain in this Sb film is similarly aligned as the up-pointing Sb islands in Figure 3f. In other words, the Sb film originates from the Sb islands, rather than Sb sheets, that form at the initial growth stage. This is a reasonable assessment because Sb islands grow faster than Sb sheets, as observed from the AFM height measurement shown in Figure 1f. At some growth stage, the merging of Sb islands may terminate the growth of Sb sheets. This explains the disappearance of the orientation representing Sb sheets in this thick Sb film. In fact, the observation here echoes the schematic arrangement shown in Figure 3f, where the atomic arrangement of Sb islands on graphene seems to be more energetically favorable. Figure 4g shows the azimuthal scan of Sb $(10\bar{1}1)$ at χ = 72°. An average fwhm of 2.3° is obtained, indicating the spread of Sb grains in the in-plane orientation is small in this film, too. All evidence in Figure 4 demonstrates a high crystallinity Sb thin film on the as-grown graphene.

DOI: 10.1021/acsnano.8b02374
ACS Nano 2018, 12, 6100–6108

Sb Thin Films on the Transferred Graphene. Figure 4 also shows SEM and XRD results obtained from a 300 nm thick Sb film deposited on a transferred graphene at 150 °C. SEM images of this film shown in Figure 4b present highly crystalline morphology. The inset in Figure 4b shows that there are small dark spots on the surface of this film. This may be associated with oxidation of Sb, which will be discussed in the Raman Scans of Sb Products and Graphene underneath Sb section. XRD θ–2θ scan shown in Figure 4c presents a similar diffraction of Sb as the counterpart grown on as-grown graphene; that is, the film is (0001) oriented along the out-of-plane direction. The rocking curve of Sb (0003) is shown in Figure 4d with a fwhm of 1.26°. Compared to the Sb film on the as-grown graphene, the spread of the grains in the Sb film along the out-of-plane direction is larger, but overall the dispersion is still small. Figure 4f shows the X-ray pole figure of Sb $(10\bar{1}1)$ film on a transferred graphene, using the same conditions as those in Figure 4e. Again, six sharp and symmetrical poles are found at $\chi = 72°$. This implies that the texture of this film is similar to that of the Sb thin film grown on the as-grown graphene. It should be stressed that this piece of data is solid evidence demonstrating that Sb indeed is epitaxially grown on graphene because the material underneath the graphene is amorphous SiO_2, which is unlikely to induce epitaxy of Sb. Figure 4g shows the azimuthal scan of Sb $(10\bar{1}1)$ at $\chi = 72°$. An average fwhm of 2.0° is obtained, indicating a small in-plane crystal dispersion. Overall, the Sb film on transferred graphene has a high crystallinity, similar to that of the Sb film grown on the as-grown graphene.

Raman Scans of Sb Products and Graphene underneath Sb. Raman spectra of three Sb samples are shown in Figure 5a. One is the ultrathin Sb, in island and sheet forms, deposited on the as-grown graphene. The other two are the Sb thin films shown in Figure 4. No Raman spectrum was collected from ultrathin Sb on transferred graphene due to the low density of Sb islands (Figure S1a). In Figure 5a, the red spectrum represents Sb islands and sheets on the as-grown graphene. E_g and A_{1g} modes of Sb can be identified. In addition, their overtone $(A_{1g} + E_g)$ in the form of a broad bump can be found around 270 cm^{-1}.[31] The blue and purple spectra represent Sb thin films on the as-grown graphene and transferred graphene, respectively. Raman modes observed in these two spectra are similar to those in the red spectrum, but their peak positions down shift slightly in comparison with those in the red spectrum, which is the result of film thickness change.[9] For Sb thin film on transferred graphene, one more type of Raman spectrum is found, shown by the green curve. Two additional peaks at 189 and 253 cm^{-1} in the green spectrum are attributed to Sb_2O_3. This implies that the sample was partially oxidized, which may also explain the dark spots observed in Figure 4b. The oxidization of this sample is speculated to be caused by the weeks-long exposure in the ambient condition after growth.

Figure 5b,c focuses on the G and 2D peaks of graphene, respectively. The Raman spectra were collected from the ultrathin Sb, in island and sheet forms, deposited on as-grown graphene. The solid curves represent spectra collected from an area that is covered with Sb, and the dashed curves represent spectra collected from an area that is free of Sb (the area was covered with sample clamps during deposition, thus no Sb was deposited). First, it is seen that G and 2D peaks of graphene can be well-resolved even with Sb on top. This is further evidence that graphene was indeed under Sb for Sb to grow. No loss of graphene occurred during a deposition. Second, the graphene peak positions do not change, regardless with or without Sb. It means no measurable strain effect in graphene after Sb deposition, as a strained graphene would have caused a peak shifting. Although graphene may have already been doped by the underlying Cu, the introduction of Sb on the top of graphene surface did not additionally dope graphene[32,33] because a change of doping level would likely have led to peak shifting, as well. Third, no disorder (D) peak of graphene is observed in either Sb-covered area or uncovered area. For a Sb-uncovered graphene, essentially, pristine as-grown graphene, it is normal that the D peak is not seen because the graphene is highly ordered in its as-grown form. In this study, the D peak is not seen even after a deposition of Sb on top of graphene, suggesting the deposition process did not create disorder in graphene. Lastly, the sharp peak at 1557 cm^{-1} in Figure 5b shows up no matter what samples are being measured, even when a scan is performed without a sample. It is thus a system artifact and should be ignored.

CONCLUSIONS

In conclusion, van der Waals epitaxy of Sb on single-crystalline graphene was demonstrated. On the as-grown graphene, it was found that the growth of ultrathin Sb followed two morphologies and growth modes, that is, Sb islands in VW mode and Sb sheets in FM mode. On the transferred graphene, in contrast, only Sb islands in the VW mode were found. This comparison suggested that Sb sheets formed on the as-grown graphene were a result of remote epitaxy between Sb and underlying Cu. Intrinsically, Sb grew on graphene in VW mode, different from the anticipation of FM mode. For relatively thicker Sb films, no substrate effect can be distinguished as the morphology, microstructure, and crystallinity were very similar for Sb films grown on as-grown and transferred graphene substrates. A crystallographic investigation using EBSD and XRD revealed two epitaxial alignments between Sb(0001) and graphene, namely, Sb $[2\bar{1}\bar{1}0]\|$graphene [10] for Sb sheets and Sb $[10\bar{1}0]\|$graphene [10] for Sb islands. For thicker Sb films, the epitaxial alignment between Sb(0001) and graphene was found to be the same as those of Sb islands on graphene. This was true for both Sb films on as-grown and transferred graphene substrates. Raman spectroscopy indicated that the graphene under Sb was not affected by the deposition of Sb, supported by no peak shifting (thus, no strain or doping effect) or emergence of disorder peak after the growth of Sb on graphene. The interface formation of Sb on graphene revealed in this study could provide guidance to explore the interaction between antimonene and graphene in the future.

EXPERIMENTAL METHOD

Single-crystalline Cu(111) films were grown on *c*-sapphire wafers (10 mm × 10 mm × 0.5 mm, MTI Corp.) using DC sputtering. Single-crystalline graphene was then grown on the Cu(111)/sapphire substrates using low-pressure CVD. The graphene was transferred to SiO_2(50 nm)/Si substrates using the standard poly(methyl methacrylate)-mediated wet method. Details regarding these procedures and characterization confirming the single crystallinity of graphene can be found elsewhere.[29] The transferred graphene on SiO_2(50 nm)/Si was annealed in vacuum (50 mTorr) in a forming gas (95% Ar and 5% H_2) at 550 °C for 1 h. After being annealed, the transferred graphene was immediately loaded into a vacuum chamber for Sb deposition. The base pressure of the chamber was maintained at the low end of 10^{-7} Torr. Sb granules (Sigma-Aldrich) in an alumina crucible were heated up in a tungsten wire basket. Two types of substrates were used, as-

DOI: 10.1021/acsnano.8b02374
ACS Nano 2018, 12, 6100–6108

grown graphene on Cu(111)/*c*-sapphire and transferred graphene on SiO_2(50 nm)/Si substrates. The deposition rate was maintained at ~3 Å/s, monitored with a QCM. The substrate temperature for Sb deposition was varied from room temperature to 300 °C on transferred graphene on SiO_2/Si. It was found that at room temperature Sb nucleated in a worm-like island feature without regular-shaped crystalline facets, a sign of inferior crystallinity, shown in Figure S3. On the other hand, nucleation of Sb on graphene became nearly impossible when the substrate temperature was higher than 200 °C. We speculate that it is related to the decreasing sticking coefficient of Sb (melting point at 630.6 °C under atmospheric pressure) with increasing substrate temperature. As a result, the substrate temperature of 150 ± 10 °C was selected as the default.

SEM images were acquired with a Carl Zeiss SUPRA 55 SEM system. AFM images were scanned with a PSI XE100 AFM in noncontact mode. EBSD was collected with a NordlysNano detector (Oxford Instruments) integrated with a Carl Zeiss Ultra 1540 SEM/FIB system. The crystallographic orientation data were collected using the Aztec EBSD data acquisition software and postanalyzed using the HKL Channel 5 package for crystallographic orientation mapping and pole figure/inverse pole figure plotting. XRD was measured with a Bruker D8 Discover X-ray diffractometer (Cu Kα = 1.54 Å). The beam and detector slits for XRD were both 0.6 mm. For X-ray pole figure acquisition, the range and step size of azimuthal angle (φ) were 0−359 and 1°, respectively; the range and step size of polar angle (χ) were 0−88 and 2°, respectively. For the crystallographic interpretation, including both EBSD and XRD, two-index, three-index, and four-index were used for graphene, Cu, and Sb, respectively. Raman spectra were acquired with a Renishaw 2000A spectrometer configured in backscattering mode. The excitation source was a 514 nm Ar ion laser line without polarization. Laser power, integration time, and grating for this spectrometer were 10 mW, 20 s, and 2400 grooves/mm, respectively.

ASSOCIATED CONTENT

Supporting Information

The Supporting Information is available free of charge on the ACS Publications website at DOI: 10.1021/acsnano.8b02374.

Additional SEM and EBSD data (PDF)

AUTHOR INFORMATION

Corresponding Author

*E-mail: sunx12@rpi.edu.

ORCID

Xin Sun: 0000-0001-5633-3371

Zonghuan Lu: 0000-0003-2375-8247

Yiping Wang: 0000-0001-7626-3278

Jian Shi: 0000-0003-2115-2225

Notes

The authors declare no competing financial interest.

ACKNOWLEDGMENTS

This work was supported by the NYSTAR Focus Center at RPI, C130117 and Rensselaer. We also acknowledge NSF award CMMI 1635520. The authors wish to thank Prof. Nikhil Koratkar for offering the CVD furnace. The authors also acknowledge Micro and Nano Fabrication Clean Room (MNCR) staff at RPI for facilitating part of the experimental work.

REFERENCES

(1) Singh, D.; Gupta, S. K.; Sonvane, Y.; Lukacevic, I. Antimonene: A Monolayer Material for Ultraviolet Optical Nanodevices. *J. Mater. Chem. C* **2016**, *4*, 6386−6390.

(2) Ersan, F.; Aktürk, E.; Ciraci, S. Stable Single-Layer Structure of Group-V Elements. *Phys. Rev. B: Condens. Matter Mater. Phys.* **2016**, *94*, 245417.

(3) Rudenko, A. N.; Katsnelson, M. I.; Roldán, R. Electronic Properties of Single-Layer Antimony: Tight-Binding Model, Spin-Orbit Coupling, and the Strength of Effective Coulomb Interactions. *Phys. Rev. B: Condens. Matter Mater. Phys.* **2017**, *95*, 081407.

(4) Pizzi, G.; Gibertini, M.; Dib, E.; Marzari, N.; Iannaccone, G.; Fiori, G. Performance of Arsenene and Antimonene Double-Gate Mosfets from First Principles. *Nat. Commun.* **2016**, *7*, 12585.

(5) Zhang, S.; Yan, Z.; Li, Y.; Chen, Z.; Zeng, H. Atomically Thin Arsenene and Antimonene: Semimetal−Semiconductor and Indirect−Direct Band-Gap Transitions. *Angew. Chem., Int. Ed.* **2015**, *54*, 3112−3115.

(6) Wang, Y.; Huang, P.; Ye, M.; Quhe, R.; Pan, Y.; Zhang, H.; Zhong, H.; Shi, J.; Lu, J. Many-Body Effect, Carrier Mobility, and Device Performance of Hexagonal Arsenene and Antimonene. *Chem. Mater.* **2017**, *29*, 2191−2201.

(7) Kim, S. H.; Jin, K.-H.; Park, J.; Kim, J. S.; Jhi, S.-H.; Yeom, H. W. Topological Phase Transition and Quantum Spin Hall Edge States of Antimony Few Layers. *Sci. Rep.* **2016**, *6*, 33193.

(8) Ares, P.; Aguilar-Galindo, F.; Rodríguez-San-Miguel, D.; Aldave, D. A.; Díaz-Tendero, S.; Alcamí, M.; Martín, F.; Gómez-Herrero, J.; Zamora, F. Mechanical Isolation of Highly Stable Antimonene under Ambient Conditions. *Adv. Mater.* **2016**, *28*, 6332−6336.

(9) Ji, J.; Song, X.; Liu, J.; Yan, Z.; Huo, C.; Zhang, S.; Su, M.; Liao, L.; Wang, W.; Ni, Z.; Hao, Y.; Zeng, H. Two-Dimensional Antimonene Single Crystals Grown by Van Der Waals Epitaxy. *Nat. Commun.* **2016**, *7*, 13352.

(10) Gibaja, C.; Rodriguez-San-Miguel, D.; Ares, P.; Gómez-Herrero, J.; Varela, M.; Gillen, R.; Maultzsch, J.; Hauke, F.; Hirsch, A.; Abellán, G.; Zamora, F. Few-Layer Antimonene by Liquid-Phase Exfoliation. *Angew. Chem., Int. Ed.* **2016**, *55*, 14345−14349.

(11) Lei, T.; Liu, C.; Zhao, J.-L.; Li, J.-M.; Li, Y.-P.; Wang, J.-O.; Wu, R.; Qian, H.-J.; Wang, H.-Q.; Ibrahim, K. Electronic Structure of Antimonene Grown on Sb_2Te_3 (111) and Bi_2Te_3 Substrates. *J. Appl. Phys.* **2016**, *119*, 015302.

(12) Fortin-Deschênes, M.; Waller, O.; Menteş, T. O.; Locatelli, A.; Mukherjee, S.; Genuzio, F.; Levesque, P. L.; Hébert, A.; Martel, R.; Moutanabbir, O. Synthesis of Antimonene on Germanium. *Nano Lett.* **2017**, *17*, 4970−4975.

(13) Wu, X.; Shao, Y.; Liu, H.; Feng, Z.; Wang, Y.-L.; Sun, J.-T.; Liu, C.; Wang, J.-O.; Liu, Z.-L.; Zhu, S.-Y.; Wang, Y.-Q.; Du, S.-X.; Shi, Y.-G.; Ibrahim, K.; Gao, H.-J. Epitaxial Growth and Air-Stability of Monolayer Antimonene on $PdTe_2$. *Adv. Mater.* **2017**, *29*, 1605407.

(14) Shao, Y.; Liu, Z.-L.; Cheng, C.; Wu, X.; Liu, H.; Liu, C.; Wang, J.-O.; Zhu, S.-Y.; Wang, Y.-Q.; Shi, D.-X.; Ibrahim, K.; Sun, J.-T.; Wang, Y.-L.; Gao, H.-J. Epitaxial Growth of Flat Antimonene Monolayer: A New Honeycomb Analogue of Graphene. *Nano Lett.* **2018**, *18*, 2133−2139.

(15) Geim, A. K.; Grigorieva, I. V. Van Der Waals Heterostructures. *Nature* **2013**, *499*, 419−425.

(16) Novoselov, K. S.; Falko, V. I.; Colombo, L.; Gellert, P. R.; Schwab, M. G.; Kim, K. A Roadmap for Graphene. *Nature* **2012**, *490*, 192−200.

(17) Vlassiouk, I. V.; Stehle, Y.; Pudasaini, P. R.; Unocic, R. R.; Rack, P. D.; Baddorf, A. P.; Ivanov, I. N.; Lavrik, N. V.; List, F.; Gupta, N.; Bets, K. V.; Yakobson, B. I.; Smirnov, S. N. Evolutionary Selection Growth of Two-Dimensional Materials on Polycrystalline Substrates. *Nat. Mater.* **2018**, *17*, 318−322.

(18) Storck, P.; Vorderwestner, M.; Kondratyev, A.; Talalaev, R.; Amamchyan, A.; Woelk, E. Antimony Surfactant for Epitaxial Growth of Sige Buffer Layers at High Deposition Temperatures. *Thin Solid Films* **2010**, *518*, S23−S29.

(19) Portavoce, A.; Berbezier, I.; Ronda, A. Effect of Sb on Si/Si and Ge/Si Growth Process. *Mater. Sci. Eng., B* **2003**, *101*, 181−185.

(20) Zhang, Y.; Zhu, J. Surfactant Antimony Enhanced Indium Incorporation on Ingan (000−1) Surface: A Dft Study. *J. Cryst. Growth* **2016**, *438*, 43−48.

(21) Anyebe, E. A.; Rajpalke, M. K.; Veal, T. D.; Jin, C. J.; Wang, Z. M.; Zhuang, Q. D. Surfactant Effect of Antimony Addition to the Morphology of Self-Catalyzed $InAs_{1-X}$ Sb_X Nanowires. *Nano Res.* **2015**, *8*, 1309−1319.
(22) Pei, C. W.; Turk, B.; Héroux, J. B.; Wang, W. I. Gan Grown by Molecular Beam Epitaxy with Antimony as Surfactant. *J. Vac. Sci. Technol., B: Microelectron. Process. Phenom.* **2001**, *19*, 1426−1428.
(23) Park, K.-H.; Ha, J. S.; Yun, W. S.; Lee, E.-H. Self-Organization of Uniform Ag Nano-Clusters on Sb-Terminated Si(100) Surface. *Surf. Sci.* **1998**, *415*, 320−327.
(24) Pachinger, D.; Groiss, H.; Teuchtmann, M.; Hesser, G.; Schäffler, F. Surfactant-Mediated Si Quantum Dot Formation on Ge(001). *Appl. Phys. Lett.* **2011**, *98*, 223104.
(25) Adam, N. K. *The Physics and Chemistry of Surfaces*, 3rd ed.; Oxford University Press, 1941.
(26) Wang, S.; Zhang, Y.; Abidi, N.; Cabrales, L. Wettability and Surface Free Energy of Graphene Films. *Langmuir* **2009**, *25*, 11078−11081.
(27) Dlubak, B.; Kidambi, P. R.; Weatherup, R. S.; Hofmann, S.; Robertson, J. Substrate-Assisted Nucleation of Ultra-Thin Dielectric Layers on Graphene by Atomic Layer Deposition. *Appl. Phys. Lett.* **2012**, *100*, 173113.
(28) Nguyen, N. N.; Jo, S. B.; Lee, S. K.; Sin, D. H.; Kang, B.; Kim, H. H.; Lee, H.; Cho, K. Atomically Thin Epitaxial Template for Organic Crystal Growth Using Graphene with Controlled Surface Wettability. *Nano Lett.* **2015**, *15*, 2474−2484.
(29) Lu, Z.; Sun, X.; Xiang, Y.; Washington, M. A.; Wang, G.-C.; Lu, T.-M. Revealing the Crystalline Integrity of Wafer-Scale Graphene on SiO_2/Si: An Azimuthal RHEED Approach. *ACS Appl. Mater. Interfaces* **2017**, *9*, 23081−23091.
(30) Kim, Y.; Cruz, S. S.; Lee, K.; Alawode, B. O.; Choi, C.; Song, Y.; Johnson, J. M.; Heidelberger, C.; Kong, W.; Choi, S.; Qiao, K.; Almansouri, I.; Fitzgerald, E. A.; Kong, J.; Kolpak, A. M.; Hwang, J.; Kim, J. Remote Epitaxy through Graphene Enables Two-Dimensional Material-Based Layer Transfer. *Nature* **2017**, *544*, 340−343.
(31) Wang, X.; Kunc, K.; Loa, I.; Schwarz, U.; Syassen, K. Effect of Pressure on the Raman Modes of Antimony. *Phys. Rev. B: Condens. Matter Mater. Phys.* **2006**, *74*, 134305.
(32) Walter, A. L.; Nie, S.; Bostwick, A.; Kim, K. S.; Moreschini, L.; Chang, Y. J.; Innocenti, D.; Horn, K.; McCarty, K. F.; Rotenberg, E. Electronic Structure of Graphene on Single-Crystal Copper Substrates. *Phys. Rev. B: Condens. Matter Mater. Phys.* **2011**, *84*, 195443.
(33) Marsden, A. J.; Asensio, M.-C.; Avila, J.; Dudin, P.; Barinov, A.; Moras, P.; Sheverdyaeva, P. M.; White, T. W.; Maskery, I.; Costantini, G.; Wilson, N. R.; Bell, G. R. Is Graphene on Copper Doped? *Phys. Status Solidi RRL* **2013**, *7*, 643−646.

DOI: 10.1021/acsnano.8b02374
ACS Nano 2018, 12, 6100−6108